

# Recovering Spatiotemporal Correspondence between Deformable Objects by Exploiting Consistent Foreground Motion in Video

Luca Del Pero<sup>1</sup>

ldelper@inf.ed.ac.uk

Susanna Ricco<sup>2</sup>

ricco@google.com

<sup>1</sup>University of Edinburgh

Rahul Sukthankar<sup>2</sup>

sukthankar@google.com

<sup>2</sup>Google Research

Vittorio Ferrari<sup>1</sup>

ferrari@inf.ed.ac.uk

## Abstract

Given unstructured videos of deformable objects (such as animals in the wild), we automatically recover spatiotemporal correspondences to map one object to another. In contrast to traditional methods based on appearance, which fail in such challenging conditions, we exploit consistency in observed object motion between instances. Our approach discovers pairs of short video intervals where the foreground moves in a consistent manner and uses these candidates as seeds for spatial alignment. We model the spatial correspondence between point trajectories generated by an object in one interval to those in the other using a homography. We find thousands of pairs of frames for which we successfully recover valid alignments without any human supervision.

## 1. Introduction

Most computer vision systems cannot take advantage of the abundance of Internet video content as training data. This is because current algorithms typically learn only under strong supervision and annotating video content is labor intensive. Our work is motivated by recent efforts to learn visual concepts from large quantities of weakly/noisily labeled video [19, 22, 25, 30]. Here, we explore a slightly different question: can we reliably recover spatiotemporal correspondences between deformable objects under weak supervision? For instance, given a collection of animal documentary videos, can we automatically match pixels on a tiger in one video to those on a different tiger in another video (Figs. 1 and 2)?

Recovering point-to-point spatiotemporal correspondences across videos is powerful because it enables us to assemble a collection of *aligned* foreground masks (automatically extracted) from a collection of videos of the same object class. For instance, in Fig. 1, we can map each part of a tiger in the first video to the corresponding part in the second (e.g. head goes to head, front-right paw goes to



Figure 1. We recover point-to-point spatiotemporal correspondences across a collection of unstructured videos of deformable objects, for example, tigers in the wild. Here, we display the recovered correspondences by mapping tigers from frames in two different videos (top) onto each other (bottom). A key feature of this work is the use of motion cues to find short video intervals where the foreground moves in a consistent manner. This enables finding correspondences despite large variations in appearance (e.g., the white and orange tiger here).

front-right paw, etc.). Accomplishing this task in the presence of significant object appearance variations is particularly important since it enables the collection to capture the richness of the visual concept (e.g., different coloring and textures of an animal, like in Figs. 1 and 2). Achieving this could replace the expensive manual annotations required by several popular methods for learning visual concepts [7, 10, 14, 31, 34], including methods that require annotations at the part level [1, 3, 11]. Additionally, it can enable novel applications, such as replacing one instance of an object with a suitable instance from a different video (like the adult tiger and the cub in Fig. 2, bottom).

Our task is challenging because real-world videos are not temporally segmented and contain multiple moving objects filmed against cluttered backgrounds under varying viewpoints, as well as occlusions and camera motion. Traditional methods for matching still images using local appear-

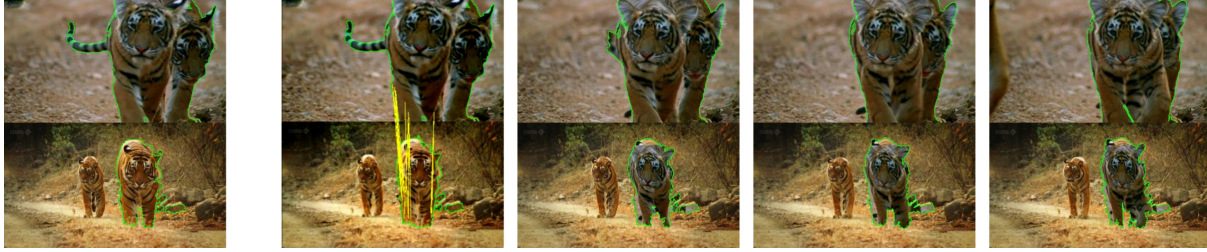


Figure 2. Pairs of short sequences in different videos with consistent foreground motion can be matched more reliably than individual frames. Here, the two sequences are aligned in time (frames are in one-to-one correspondence) and space (2D points are in correspondence). Our method recovers the spatial alignment from such pairs by fitting a homography to dense trajectory correspondences, shown in yellow in the second column (note the correspondences between trajectories on the legs of the two walking tigers). In the last three columns, we display the alignment by projecting the pixels in the first video (top) onto the second (bottom) with the recovered homography. An estimate of the foreground (found automatically using motion cues) provides the spatial support for the alignment (shown in green). Using trajectories enables us to align instances despite large differences in appearance, like matching the cub to the adult tiger here.

ance descriptors [2, 16, 21] typically fail on this data, *i.e.*, they do not find reliable correspondences across individual frames from different videos. Instead, this can be done more reliably by matching motion descriptors across temporal intervals where the objects exhibit consistent motion patterns, which is the key observation behind this work. In other words, we can exploit the characteristic motion of an object class (*e.g.*, a tiger’s prowl) to identify suitable correspondences, as well as to align them with great accuracy. To do so, we introduce a new technique that aligns sequences of frames spatiotemporally by using matches between point trajectories (*e.g.*, those computed as in Wang *et al.* [32]) in contrast to aligning still images by matching appearance-based keypoints [21, 23]).

The contributions of our work can be summarized as follows. First, we propose a weakly supervised system that goes from a large collection of unstructured video containing an instance of the object class to a tight network of spatiotemporal correspondences. Second, we introduce an appearance-free method for aligning sequences of frames with consistent motion based on trajectory matching. Third, we make publicly available a new set of ground-truth annotations: 19 landmark positions (*e.g.*, left eye, front left knee, neck, etc.) for each tiger in over 17,500 frames of animal documentary footage. Our experiments show that exploiting consistency in foreground motion as proposed here significantly outperforms traditional approaches for recovering correspondence based on local appearance matching [23]. Our method recovers over 1000 pairs of correctly aligned sequences from 100 video shots of tigers in the wild (roughly 12 minutes of video). We emphasize that the recovered alignment is between entire sequences (*e.g.*, Fig. 2), not just pairs of frames. If we count the frames in the aligned sequences individually, our method puts in correspondence 10,000 pairs of frames. At the same level of precision (0.5), local appearance matching using SIFT key-

points returns fewer than 3000 pairs of frames.

## 2. Related work

Most works on spatial alignment focus on matching between images for a variety of applications such as multi-view reconstruction [29], image stitching [4], and object instance recognition [12, 23]. The traditional approach identifies candidate matches using a local appearance descriptor (*e.g.*, SIFT [23]) with global geometric verification performed using RANSAC [6, 13] or semi-local consistency checks [12, 18, 28]. Patchmatch [2] and SIFT flow [21] generalize this notion to match patches between semantically similar scenes.

Spatiotemporal alignment [5] and temporal frame correspondence [27] in video has also been explored, but typically only for multiple viewpoints of the same dynamic scene. Similarly, Fan *et al.* [9] demonstrated alignment of presentation video to presentation slides by exploiting the foreknowledge that the two are in correspondence. In the context of video action recognition, there has been work on matching of spatiotemporal templates to actor silhouettes [15, 35] or groupings of supervoxels [20]. Our work is quite different because we map pixels from one unstructured video to another. Jain *et al.* [17] mine discriminative space-time patches and match these across videos. Their work focuses on rough alignment using sparse matches (typically one patch per clip) while we seek a finer spatial alignment driven by dense correspondences between trajectories, which leads to an accurate homography estimation.

A few recent works exploit video as a source of training data for object class detectors [25, 30]. However, their use of video is limited to segmenting objects from their background. Ramanan *et al.* [26] build a simple 2D pictorial structure model of an animal from one video. None of these methods find spatiotemporal correspondences between object instances.

### 3. Overview

The input to our method is a large set of video shots, each containing one or more instances of an object class (*e.g.*, tiger). The output is a collection of pairwise correspondences between frames, like the one in Fig. 1. Each correspondence is both temporal, *i.e.* we find correspondences between individual frames from shots that are not temporally aligned, and spatial, *i.e.* we recover the transformation mapping points in the first frame to the second (Fig. 1, bottom).

We reliably recover the frame-to-frame correspondences by finding and aligning short sequences of frames that exhibit consistent foreground motion, such as the two tigers in Fig. 2. Two aligned sequences of length  $k$  provide  $k$  frame-to-frame correspondences. Aligning sequences using *motion* cues is in fact more reliable than aligning individual frames using appearance cues. The latter typically fails in the presence of clutter, occlusions, and different view-points (all common in the broad range of videos in our data). Motion also enables us to put in correspondence instances with different color and textures (like the white and orange tiger in Fig. 1, or the cub and the adult in Fig. 2). Additionally, it allows us to reliably segment the object from the background [24], which simplifies finding spatial correspondences.

**Consistent motion pairs.** We focus on automatically recovering pairs of sequences of the same length that can be aligned by a single homography transformation constant through time (*i.e.* the same homography maps the  $k$ th frame in the first sequence to the  $k$ th frame in the second sequence,  $\forall k$ ). We call such a pair of sequences a *Consistent Motion Pair* (CMP). From this definition it follows that only two sequences where the object is performing similar motions in the same order can be a CMP. This includes sequences with non-rigid deformations, as long as the deformations occur in the same order. For example, the two tigers in Fig. 2 are in the same phase of walking.

**System architecture.** Our method deems two sequences to be a CMP if it can estimate a homography geometrically consistent with trajectory correspondences extracted across the sequences. However, naively examining every possible pair of sequences in the data is impractical. For example, the number of pairs of fixed length in just 20 minutes of video (30,000 frames) is roughly one billion. Hence, we propose a fast scheme for identifying a manageable set of promising CMP candidates (steps 1-4 in Fig. 3). This allows us to process a large number of shots with a limited computational budget. We provide details in Sec. 4. Then, we only retain a candidate if our method can estimate a geometrically consistent homography (step 5 in Fig. 3), which is more computationally intensive (Sec. 5). For each retained candidate, we output the  $k$  associated frame-to-frame corre-

spondences together with the estimated homography. Note that as preprocessing we use the method by Papazoglou *et al.* [24] to extract reliable foreground masks from each shot based on motion. These masks remove confusing evidence from the background.

### 4. Extracting CMP candidates

We now present how to extract CMP candidates from all the possible pairs of sequences in a database of video shots. First, we use the method in [8] to recover clusters of short intervals showing similar motion. This method first segments the input shots into shorter intervals (Fig. 3, step 2) and clusters them using motion cues (Fig. 3, step 3). As discussed in [8], clustering shorter intervals (typically 10 – 200 consecutive frames in a shot each) finds more compact clusters than directly clustering the entire shots.

We then extract a small set of CMP candidates from each pair  $(p, q)$  of intervals within a cluster (Fig. 3, step 4). First, we compute a frame-level representation by aggregating in a bag of words (BoW) all of the descriptors formed by trajectories (*e.g.*, trajectory shape [32]) starting at that frame, as shown in Fig. 4. Let  $d_{ij}$  be the histogram intersection between the BoWs for frame  $i$  in  $p$  and frame  $j$  in  $q$ . We generate CMP candidates by finding the closest sequences of  $k$  frames, ranked using

$$s([f_i^p, f_{i+k-1}^p], [f_j^q, f_{j+k-1}^q]) = \sum_{l=0}^{k-1} d_{(i+l)(j+l)}. \quad (1)$$

This distance preserves the temporal order of the frames, whereas using a BoW aggregated over the sequences would not. The top ten candidates from each pair of intervals are passed on to the next processing step (Sec. 5).

The naive way of computing (1) for every pair of sequences in the dataset (*i.e.*, without doing any clustering) is quadratic in the number of frames in the dataset. Clustering reduces the search space to quadratic in the number of frames *within a cluster*. The clustering step itself is very efficient, as it only requires computing distances between pairs of intervals, which is orders of magnitude fewer than every pair of frames. We show in the experiments that this procedure extracts CMP candidates with good accuracy (Sec. 6.2). On our dataset, it effectively reduces the number of homographies we need to compute from 300 million to 3000.

### 5. Spatial alignment estimation

We now discuss how we estimate the homography for a CMP candidate found in the previous step. A standard method to estimate a homography between two images is to apply RANSAC on a set of putative keypoint correspondences [16].



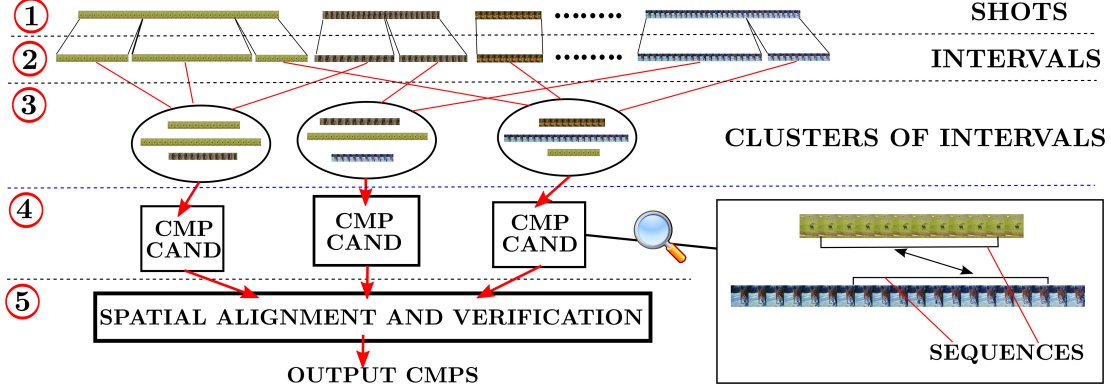


Figure 3. Overview of our method. The input is a collection of shots showing the same class (1). Each shot (which can be of any length) is partitioned into shorter temporal intervals of 10-200 frames (2), which are then clustered together (3) using motion cues. ([8] shows that using intervals shorter than the original shots finds more compact clusters.) The clusters effectively limit the search space: we extract CMP candidates only from pairs of intervals in the same cluster (4). For each pair, we extract CMP candidates from all possible pairs of sequences of fixed length (10 frames). An example of a pair is shown in the bottom right (see text and Fig. 4 for the details). Last, we estimate a spatial alignment for each candidate (5) using point correspondences found using motion cues (see text) and output only those candidates where the alignment is geometrically consistent with the correspondences.

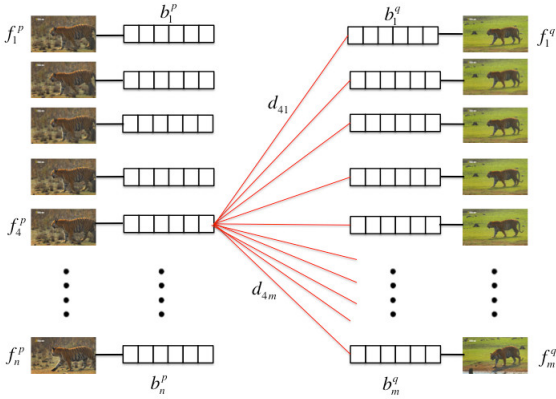


Figure 4. Generating CMP candidates between two intervals. First, we approximate the pairwise distance between frames as the histogram distance between their BoWs (which contains all motion descriptors through the frame). Then we keep as CMP candidates the top scoring pairs of sequences of length  $k$  with respect to (1). Note that for the two intervals above, the number of pairs of sequences to examine is  $(n - k) \cdot (m - k)$ .

A 2D planar homography  $H_{uv}$  between two images can be determined from a set of four or more correspondences by solving

$$X_u = H_{uv} X'_v \quad (2)$$

where  $X_u \leftrightarrow X_v$  denote the point correspondences (see the Normalized DLT algorithm for more details [16]). RANSAC is an iterative random algorithm that estimates a homography from a set of putative correspondences  $\mathcal{P}_{uv} = \{(x_u, y_u) \leftrightarrow (x_v, y_v)\}$  that may include outliers. Tradition-

ally,  $\mathcal{P}_{uv}$  contains matches between local appearance descriptors, like SIFT [23]. At each iteration, a hypothesis is generated by fitting a homography to four correspondences randomly sampled from  $\mathcal{P}_{uv}$ ; the computed homography with the largest number of inliers is kept. The final ratio of inliers to outliers can be used to discard the output homography (*i.e.*, if this number is below a given threshold). This final consistency check *filters out* homographies that do not fit enough correspondences.

We modify this algorithm in two significant ways. First, we use point correspondences found by matching trajectories. The motion descriptors of the trajectories prove much more robust than SIFT keypoints (see the results in Fig. 10). Second, the algorithm above is used to align still images, while we match the two sequences of a CMP candidate. Under the assumption that the homography does not change with time, a straightforward modification would be to aggregate all point correspondences in a sequence in  $\mathcal{P}_{uv}$ . However, this does not preserve any temporal information. Hence, we propose a new method to estimate a homography from matched trajectories that preserves the temporal order of their points.

Finding matches between trajectories is discussed next (Sec 5.1). We then discuss fitting homographies to matched trajectories (Sec 5.2). Last, we make this method more robust by adding correspondences between the estimated foreground masks (Sec. 5.3).

### 5.1. Matching trajectories

We now discuss finding matches between trajectories from the two sequences of a CMP candidate (extracted using the dense point tracker by Wang *et al.* [32]). We match

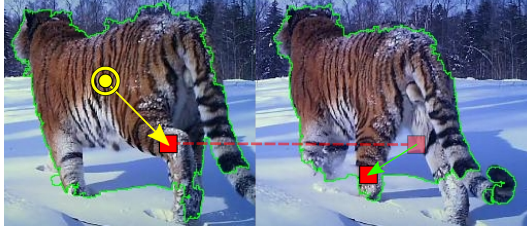


Figure 5. Modifying the TS descriptor. The TS descriptor is the concatenation of the 2D displacement vectors of the trajectory across consecutive frames (the green arrow denotes one such vector). This descriptor works well when aggregated in unordered representations like Bag-of-Words [32], but matches found between individual trajectories are not very robust. We make TS more discriminative by appending the vector (in yellow) between the trajectory and the center of mass of the foreground mask (in green) in the frame where the trajectory starts.

each trajectory in the first sequence to its nearest neighbor in the second with respect to Euclidean distance. We then only return matches where the ratio between the distance to the nearest neighbor and that to the second-nearest is above a threshold [23]. We use trajectories that are ten frames long and only match those that start in the same frame in both sequences. Note that a correspondence between two such trajectories provides ten point-to-point correspondences (one per frame).

The descriptor we use for matching is a modification of the Trajectory Shape (TS) descriptor [33]. The original descriptor is the concatenation of the 2D displacement vectors of a trajectory, normalized by the total displacement, and is entirely appearance-free (hence, it can match trajectories from instances that look different, like the adult and the cub in Fig. 2). However, matches found based on the TS descriptor are often not reliable, especially in the presence of large foreground regions that move uniformly. For example, most trajectories on the torso of a tiger walking (like the one in Fig 5) have a very similar motion, and their TS descriptors are almost identical. Appending to TS the vector between the trajectory position and the center of mass of the foreground mask (Fig. 5) in the frame where the trajectory starts provides more reliable matches. To ensure we can match objects at different scales, we normalize the vector by the diagonal of the bounding box enclosing the segmentation mask. The low dimensionality of this descriptor (20 for trajectories of length 10) allows us to find matches efficiently.

## 5.2. Homography from trajectory matches

We fit a homography to the trajectory matches extracted from a CMP candidate in two different ways:

**Independent matching (IM)** Each trajectory match generates  $n$  point-to-point correspondences per frame, one

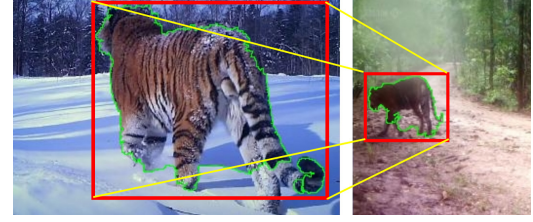


Figure 6. Spatial mapping from the foreground masks. Consider the smallest possible box (in red) containing the foreground mask (in green). The correspondences between the corners (in yellow) provide a straightforward spatial mapping.

for each point in the trajectory. Each point correspondence is used independently during RANSAC.

**Temporal matching (TM)** We sample four *trajectory* matches at each RANSAC iteration instead of four point correspondences. We solve Eq. 2 using the  $4n$  associated point correspondences; the overdetermined system is solved in the least squares sense. A trajectory match is considered an inlier only if  $\frac{n}{2} + 1$  of its point correspondences are inliers. We found empirically that this works better than enforcing all points to be inliers.

Temporal matching encourages geometric consistency over the duration of the CMP candidate. Independent matching can potentially overfit to point correspondences from just a few frames. For example, all inliers could come from, say, the first frame (Fig. 11).

## 5.3. Combining trajectories with foreground masks

The homography estimated from trajectory matches tends to be inaccurate when the input matches do not cover the entire foreground. Consider the first row of Fig. 7: the homography that best fits the trajectory matches is suboptimal for the regions of the tiger without any match (it completely misaligns the tigers' left leg). To address this issue, we note that the bounding boxes enclosing the foreground masks provide a coarse, global mapping (Fig. 6). We use this as a spatial regularizer.

Specifically, we fit a homography by minimizing an objective function that uses the matches between the corners of the bounding boxes (foreground matches) as additional point-to-point correspondences (four per frame in a CMP):

$$\min \|H_{uv}X'_v - X_u\| + \lambda \|H_{uv}F'_v - F_u\| \quad (3)$$

$F_u$  and  $F_v$  denote the foreground matches, while  $X_u$  and  $X_v$  denote the four trajectory matches that are randomly sampled at every RANSAC iteration. By setting  $\lambda = 0$  we obtain the same objective function as before. With  $\lambda > 0$ , our method is much more stable (see the improved alignment in Fig. 7, bottom right). We conclude noting that

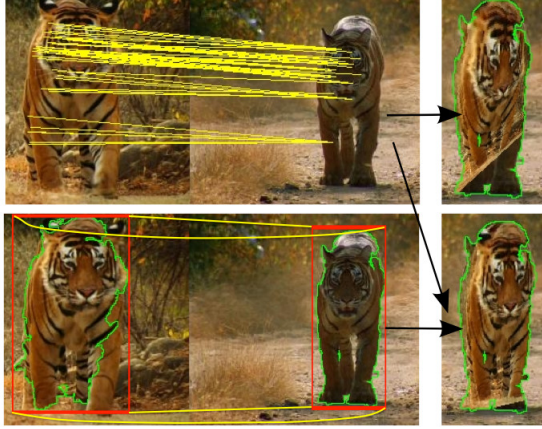


Figure 7. Top: Trajectory correspondences (in yellow) often cover only part of the object (head and right leg here). Here, RANSAC overfit to the correspondences on the head, and the estimated homography provides an incorrect mapping for the legs (top right). Bottom: Adding correspondences from the foreground bounding boxes provides a more stable mapping (bottom right). Note that correspondences in the bottom row are also found automatically by our method; there is no manual intervention needed.

the foreground correspondences fit in our pipeline of finding correspondences using motion, since motion boundaries are the most important cue used by Papazoglou *et al.* [24]. In this method, appearance partly helps segment the object from the background in one video, but we do not use it to find correspondences across videos.

## 6. Evaluation

We evaluate our method on a dataset of 110 video shots of tigers sourced from documentary nature footage, for a total of 17,500 frames (roughly 12 minutes of video).

### 6.1. Evaluation protocol

**Landmark annotations.** In each frame, we annotate the 2D location of 19 landmarks on the tiger.<sup>1</sup> Given that tigers are so deformable, we choose the following landmarks (Fig. 8): ankles (4), feet (4), knees (4), neck (1), shoulders (2), chin (1), pelvis (1), and eyes (2). We do not annotate landmarks that are occluded. These annotations are publicly available at [calvin.inf.ed.ac.uk/datasets/tiger-landmarks/](http://calvin.inf.ed.ac.uk/datasets/tiger-landmarks/).

Unlike coarser annotations, such as bounding boxes, this set of landmarks allows us to evaluate the alignment of objects with non-rigid parts with great accuracy. Consider Fig. 8 (bottom): although the global alignment looks correct, our landmarks detect that the front legs are swapped.

**Reprojection error.** Given a pair of frames and a homography, we project each landmark in the first frame onto the

<sup>1</sup>If more than one is visible, we annotate the tiger closest to the camera.

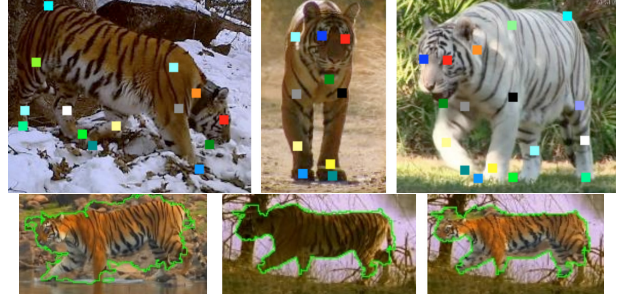


Figure 8. Examples of annotated landmarks. A total of 19 points are marked when visible in over 17,500 frames. By measuring reprojection error we can identify misaligned parts. Although the global alignment looks correct on the bottom row, the front right leg is actually mapped to the front left leg (and vice versa).

second using the homography and compute the Euclidean distance to its true location. The reprojection error is the average between this distance and the reverse (*i.e.*, the distance for landmarks projected from the second frame into the first). To avoid penalizing frames where the tiger is at a larger scale, we normalize the reprojection error by the scale of the tiger, approximated as the maximum distance between any two landmarks in the frame. The reprojection error for pairs of sequences (*e.g.*, a CMP) is the average reprojection error of all visible landmarks over all frames.

In Fig. 9 we can see that the alignment provided by the homography clearly degrades as the reprojection error grows. When the error is around 0.2, the alignment is still acceptable, but a few parts start to be misaligned. (We checked many more examples to confirm this trend.) As the error keeps increasing above 0.2, the alignment becomes significantly inaccurate. In what follows, we use this threshold to determine whether a homography estimated by our method is correct or not. However, we also require that the Intersection over Union (IoU) of the landmarks visible in the sequences is above 0.5. If the IoU is low, a homography that is globally incorrect might still map the few landmarks that are visible in both sequences correctly by chance. We show a few examples of  $\text{IoU} \leq 0.5$  in Fig. 9, caused by significantly different pose and severe cropping.

### 6.2. Evaluating CMP candidates

First, we evaluate our method for retrieving CMP candidates (Sec. 4) in isolation. Given a CMP candidate, we use its landmarks (*i.e.*, correspondences from an oracle) to fit the homography that we use to compute reprojection error. We consider a candidate valid if the resulting reprojection error is below 0.2 and IoU above 0.5.

Our method returns roughly 3000 CMP candidates. Using the criterion above, 51% are valid CMPs. Note that each CMP consists of ten aligned frames, so this result corresponds to approximately 15,000 pairs of frames that can



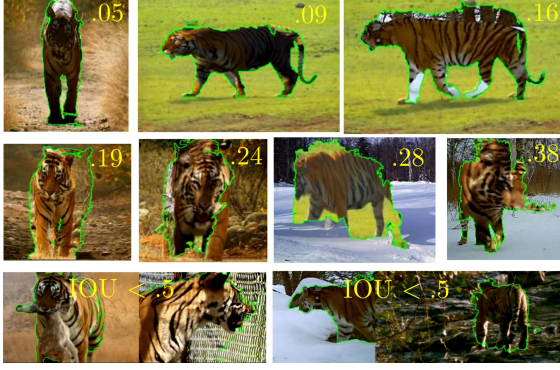


Figure 9. Reprojection error. We consider an alignment incorrect if the reprojection error computed on the ground-truth landmarks is less than 0.2. This error increases as the quality of the alignment degrades. Around 0.2 alignments contain some mistakes (*e.g.*, the slightly misaligned legs in the top row), but are typically acceptable. We reject alignments without computing the error when the Intersection over Union of the visible landmarks in the aligned pair is below 0.5 (like the two examples in the bottom row).

be spatially aligned out of 30,000. If we extract candidates by uniformly sampling sequences from pairs of shots (*i.e.*, without clustering or ranking as described in Sec. 4), the percentage of valid CMPs drops to 19%. Restricting sampling to sequences within a cluster (but without ranking) manages 47%, but it is still inferior to our full method.

### 6.3. Evaluating spatial alignment estimation

We now evaluate our method for producing the correspondences automatically. In this case, there is no oracle available to provide landmark correspondences. Since our method returns a homography for a CMP candidate when at least a given fraction of the correspondences are inliers, we can generate precision-recall curves by varying this threshold. Precision measures the fraction of CMPs returned by our method that are valid (*i.e.*, reprojection error less than 0.2 and IoU above 0.5); recall measures the fraction of CMPs we know to be valid (based on the oracle homography) for which we find a sufficiently good alignment. These curves are shown in Fig. 10.

First, we compare matching trajectories (either using independent or temporal matching) to a baseline using SIFT. The baseline fits a homography to SIFT keypoint matches found in the two sequences of the CMP candidate, using only keypoints inside the foreground mask. (Again, we preserve the temporal order by matching only keypoints in corresponding frames.) Both versions of trajectory matching are clearly superior to this SIFT baseline (Fig. 10, left). When recall is maximized for SIFT matching, we find fewer than 100 valid CMPs out of roughly 1500 returned homographies (precision is less than 0.1). In contrast, the trajectory methods match the recall of SIFT with precision near

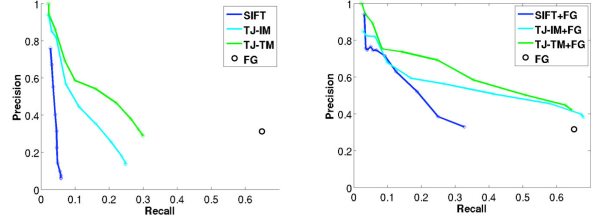


Figure 10. Left: Comparison of SIFT keypoints versus trajectory-based correspondences. Right: Results after combining SIFT or trajectory correspondences with correspondences from the foreground bounding box. Regularizing with the foreground mask improves performance for all methods. Trajectory matches outperform SIFT keypoint matches. Among the two trajectory-based methods, temporal matching (TM) is superior to independent matching (IM).

0.8. We also see that temporal matching dominates independent matching, achieving consistently higher precision for a given recall.

Adding spatial regularization using the foreground matches improves the performance of all three methods (Fig. 10, right). Again, temporal matching is superior to independent matching, and both trajectory methods outperform SIFT keypoints. We also tested an alternative that used the matches between the foreground bounding boxes alone. Note that when we use foreground matches alone we always find a homography with a large enough fraction of inliers for all values of the threshold we tested. This is because we can always find a homography that maps the four corners of a bounding box onto another exactly, and the bounding boxes did not change significantly over the duration of our CMP candidates. The best performing method is temporal matching combined with foreground correspondences: it consistently achieves higher precision for a given recall than the other combined methods and significantly improves precision compared to using the foreground correspondences alone. When recall is maximized, it returns 1500 correctly aligned CMPs (*i.e.* 15,000 pairs of frames) with precision 0.5.

Figs. 11 and 12 show the difference in quality of alignment on representative examples. Fig. 11 compares temporal matching to independent matching. In the first two columns, we show the original first and last frame of a CMP returned by our method. We map the pixels in the foreground masks of the first sequence onto the second using the homography estimated using temporal matching (top row) and independent matching (bottom row), respectively. The alignment found using temporal matching is consistently good across all ten frames, while with independent matching it degrades over time. In Fig. 12 (top rows), we show examples where combining foreground and trajectory matches is more accurate than using foreground matches

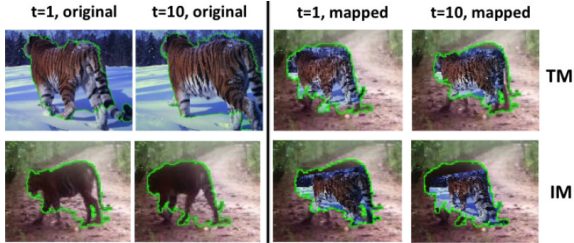


Figure 11. Temporal matching (TM) performs better than independent matching (IM). The latter often overfits to correspondences from 1-2 frames and does not provide a spatial alignment consistent through time. Here, the alignment for the first frame in the sequence is acceptable (bottom row, third column), but it degrades in the last frame (bottom row, fourth column). TM recovers an alignment that is accurate for the entire sequence (top row).

only. Without the trajectory matches included, the alignment fails when the foreground mask mistakenly includes portions of the background or excludes parts of the object. Importantly, this shows that our method can also align sequences with imperfect foreground masks. In the bottom rows, we compare the alignment found by matching SIFT keypoints to the alignment found using temporal matching for two different pairs. In each case, using trajectories finds a good alignment. SIFT instead fails, mostly because matching keypoints gets confused by the recurring texture patterns of the tigers. Consider the bottom row in particular. Although the tigers are superficially similar, the variation in the stripe pattern on the two individuals is sufficient to degrade any matching based on appearance descriptors alone. While we focus here on comparing appearance versus motion alone, we believe that the combination of appearance and motion could enable robust matching over a broader range of object classes.

## 7. Discussion

We present a method that automatically extracts dense spatiotemporal correspondences from a collection of videos showing a particular object class. We argue that motion offers a complementary modality to appearance-based descriptors for finding correspondences in video since it can: 1) segment the object of interest from cluttered backgrounds; 2) drastically prune the search space of frame pairs over which homographies need to be estimated by identifying promising short sequences; and 3) generate reliable point-to-point correspondences across such sequences from which one can accurately estimate the desired mapping.

By using the motion of dense trajectories to find pixel-level correspondences, we reliably associate parts despite variation in appearance. A tiger’s paw is recognized and matched across instances because of the characteristic way it moves as a tiger walks, not because of how it looks.

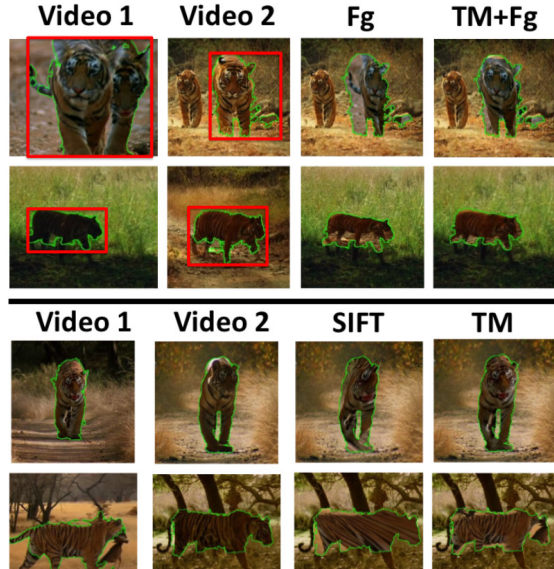


Figure 12. Top two rows: Estimating the homography from the foreground correspondences fails in several cases (third column), typically when the bounding boxes are not tight around the objects (first-second columns). However, when combined with matched trajectories, the recovered homography is accurate (fourth column). Bottom two rows: Estimating homographies from trajectory correspondences (TM) is often more accurate than from local appearance descriptors (SIFT). The striped texture confuses matches based on SIFT even when the two tigers look similar (third row).

Furthermore, trajectories that extend over multiple frames provide automatic temporal regularization as corresponding points in one frame must remain in correspondence in the surrounding frames. We use motion-based correspondences aggregated over short sequences of frames to guarantee that our method carefully selects the most reliable of the possible aligned pairs from a large amount of noisy input frames.

The correspondences we find can be used to learn a general model of the object class without requiring any human supervision beyond video-level object class labels. Additionally, they can enable novel applications, such as replacing an instance of an object with an instance from a different video, or retrieving videos in a collection that tightly match the motion of the object in a query video.

Finally, we note that although we focus here on the specific example of aligning tigers across videos, our method is not specific to this particular object class. The only requirement for success is that the objects exhibit consistency in behavior and thus exhibit the same characteristic motion patterns across different observations.

**Acknowledgments.** We are very grateful to Anestis Papazoglou for helping with the data collection, and to Shumeet Baluja for his helpful comments. This work was partly funded by a Google Faculty Research Award.



## References

- [1] H. Azizpour and I. Laptev. Object detection using strongly-supervised deformable part models. In *ECCV*, 2012. [1](#)
- [2] C. Barnes, E. Shechtman, D. Goldman, and A. Finkelstein. The generalized patchmatch correspondence algorithm. In *ECCV*, 2010. [2](#)
- [3] L. Bourdev and J. Malik. Poselets: Body part detectors trained using 3d human pose annotations. In *ICCV*, 2009. [1](#)
- [4] M. Brown and D. Lowe. Automatic panoramic image stitching using invariant features. *IJCV*, 74(1), 2007. [2](#)
- [5] Y. Caspi and M. Irani. A step towards sequence-to-sequence alignment. In *CVPR*, 2000. [2](#)
- [6] O. Chum and J. Matas. Optimal randomized ransac. *IEEE Trans. on PAMI*, 2008. [2](#)
- [7] N. Dalal and B. Triggs. Histogram of Oriented Gradients for human detection. In *CVPR*, 2005. [1](#)
- [8] L. Del Pero, S. Ricco, R. Sukthankar, and V. Ferrari. Articulated motion discovery using pairs of trajectories. *arXiv:1114.7883v1*, 2014. [3, 4](#)
- [9] Q. Fan, K. Barnard, A. Amir, and A. Efrat. Robust spatio-temporal matching of electronic slides to presentation videos. *IEEE Transactions on Image Processing*, 20(8):2315–2328, 2011. [2](#)
- [10] P. Felzenszwalb, R. Girshick, D. McAllester, and D. Ramanan. Object detection with discriminatively trained part based models. *IEEE Trans. on PAMI*, 32(9), 2010. [1](#)
- [11] P. F. Felzenszwalb and D. P. Huttenlocher. Pictorial structures for object recognition. *IJCV*, 61(1):55–79, 2005. [1](#)
- [12] V. Ferrari, T. Tuytelaars, and L. Van Gool. Simultaneous object recognition and segmentation from single or multiple model views. *IJCV*, 67(2):159–188, 2006. [2](#)
- [13] M. A. Fischler and R. C. Bolles. Random sample consensus: A paradigm for model fitting with applications to image analysis and automated cartography. *Comm. ACM*, 24(6):381–395, 1981. [2](#)
- [14] R. Girshick, J. Donahue, T. Darrell, and J. Malik. Rich feature hierarchies for accurate object detection and semantic segmentation. In *CVPR*, 2014. [1](#)
- [15] L. Gorelick, M. Blank, E. Shechtman, M. Irani, and R. Basri. Actions as space-time shapes. *IEEE Trans. on PAMI*, 29(12):2247–2253, December 2007. [2](#)
- [16] R. I. Hartley and A. Zisserman. *Multiple View Geometry in Computer Vision*. Cambridge University Press, ISBN: 0521623049, 2000. [2, 3, 4](#)
- [17] A. Jain, A. Gupta, M. Rodriguez, and L. Davis. Representing videos using mid-level discriminative patches. In *CVPR*, 2013. [2](#)
- [18] H. Jegou, M. Douze, and C. Schmid. Hamming embedding and weak geometric consistency for large-scale image search. In *ECCV*, 2008. [2](#)
- [19] A. Karpathy, S. Shetty, G. Toderici, T. Leung, R. Sukthankar, and L. Fei-Fei. Large-scale video classification with convolutional neural networks. In *CVPR*, 2014. [1](#)
- [20] Y. Ke, R. Sukthankar, and M. Hebert. Event detection in crowded videos. In *ICCV*, 2007. [2](#)
- [21] C. Liu, J. Yuen, A. Torralba, J. Sivic, and W. Freeman. SIFT Flow: Dense correspondence across different scenes. In *ECCV*, 2008. [2](#)
- [22] X. Liu, D. Tao, M. Song, Y. Ruan, C. Chen, and J. Bu. Nearest neighbor-based label transfer for weakly supervised multiclass video segmentation. In *CVPR*, 2014. [1](#)
- [23] D. Lowe. Distinctive image features from scale-invariant keypoints. *IJCV*, 60(2):91–110, 2004. [2, 4, 5](#)
- [24] A. Papazoglou and V. Ferrari. Fast object segmentation in unconstrained video. In *ICCV*, December 2013. [3, 6](#)
- [25] A. Prest, C. Leistner, J. Civera, C. Schmid, and V. Ferrari. Learning object class detectors from weakly annotated video. In *CVPR*, 2012. [1, 2](#)
- [26] D. Ramanan, A. Forsyth, and K. Barnard. Building models of animals from video. *IEEE Trans. on PAMI*, 28(8):1319 – 1334, 2006. [2](#)
- [27] C. Rao, A. Gritai, and M. Shah. View-invariant alignment and matching of video sequences. In *ICCV*, 2003. [2](#)
- [28] C. Schmid and R. Mohr. Combining greyvalue invariants with local constraints for object recognition. Technical report, INRIA Rhône-Alpes, Grenoble, France, 1996. [2](#)
- [29] S. Seitz, B. Curless, J. Diebel, D. Scharstein, and R. Szeliski. A comparison and evaluation of multi-view stereo reconstruction algorithms. In *CVPR*, 2006. [2](#)
- [30] K. Tang, R. Sukthankar, J. Yagnik, and L. Fei-Fei. Discriminative segment annotation in weakly labeled video. In *CVPR*, 2013. [1, 2](#)
- [31] P. A. Viola, J. Platt, and C. Zhang. Multiple instance boosting for object detection. In *NIPS*, 2005. [1](#)
- [32] H. Wang, A. Kläser, C. Schmid, and L. Cheng-Lin. Action Recognition by Dense Trajectories. In *CVPR*, 2011. [2, 3, 4, 5](#)
- [33] H. Wang and C. Schmid. Action recognition with improved trajectories. In *ICCV*, 2013. [5](#)
- [34] J. Wang and M. Cohen. An iterative optimization approach for unified image segmentation and matting. In *ICCV*, 2005. [1](#)
- [35] A. Yilmaz and M. Shah. Actions as objects: A novel action representation. In *CVPR*, 2005. [2](#)